

Emergent metallicity at the grain boundaries of higher-order topological insulators

Daniel J. Salib,¹ Vladimir Juričić,^{2,3} and Bitan Roy¹

¹*Department of Physics, Lehigh University, Bethlehem, Pennsylvania, 18015, USA*

²*Departamento de Física, Universidad Técnica Federico Santa María, Casilla 110, Valparaíso, Chile*

³*Nordita, KTH Royal Institute of Technology and Stockholm University, Hannes Alfvéns väg 12, SE-106 91 Stockholm, Sweden*

Topological lattice defects, such as dislocations and grain boundaries (GBs), are ubiquitously present in the bulk of quantum materials and externally tunable in metamaterials. In terms of robust modes, localized near the defect cores, they are instrumental in identifying topological crystals, featuring the hallmark band inversion at a finite momentum (translationally active type). Here we show that GB superlattices in both two- and three-dimensional translationally active higher-order topological insulators harbor a myriad of dispersive modes that are typically placed at finite energies, but always well-separated from the bulk states. However, when the Burgers vector of the constituting edge dislocations points toward the gapless corners or hinges, both second- and third-order topological insulators accommodate self-organized emergent topological metals in the GB mini Brillouin zone. We discuss possible material platforms where our proposed scenarios can be realized through band-structure and defect engineering.

Introduction. Topological lattice defects are ubiquitous in crystalline materials and are of central importance for their structural properties. In the last decade, they have emerged as viable platforms for probing topological phases of matter through a subtle interplay of the topology of the electronic wavefunctions and lattice geometry. In particular, dislocations, the defects associated with lattice translations, can probe a wide range of topological crystals featuring the band-inversion at a finite momentum directly in the bulk via the symmetry and topology protected localized defect modes either at zero [1–11] or finite [12] energy. As such, these modes are immune to interface contamination and surface termination, and have been experimentally observed in both topological crystals [13, 14] and their metamaterial analogues [15, 16].

These developments boosted the exploration of *extended* lattice defects on topological platforms, among which grain boundaries (GBs) are the most prominent ones. A GB develops at the interface between two mis-oriented crystalline grains due to the accumulated elastic stress, and at low angles, it consists of an array of dislocations [17, 18]. See Fig. 1. In turn, by virtue of the hybridization between the localized zero-energy dislocation modes, the GBs can host a wide range of quantum phases in both static [19, 20] and dynamic [21] settings, when a parent topological insulator (TI) is first-order in nature, featuring gapless modes on the edges or surfaces.

In higher-order topological insulators (HOTIs), accommodating localized states on lower-dimensional boundaries, such as hinges and corners [22–32], the dislocation modes on the other hand typically move to finite energies, controlled by the relative orientation between its Burgers vector (\mathbf{b}) and the axis of inversion (domain wall) of the discrete symmetry breaking Wilson-Dirac (WD) mass, responsible for the higher-order topology [12]. Such a nontrivial interplay between the real-space geometry of lattice defects and the momentum-space topology of WD

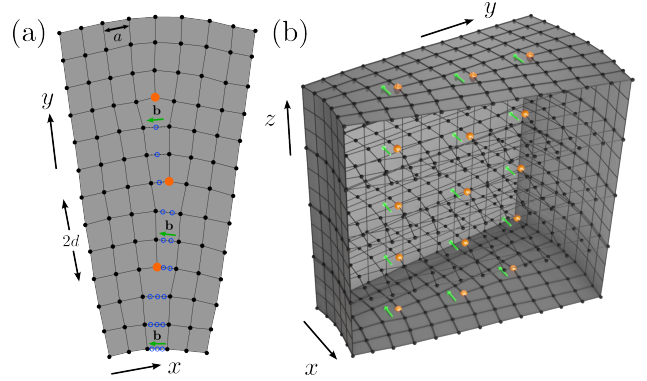


FIG. 1. Grain boundary of edge dislocations with Burgers vector $\mathbf{b} = a\mathbf{e}_x$ in (a) two and (b) three dimensions, where a is the lattice spacing. The center of individual dislocation cores are shown in orange and the missing sites are shown by open blue circles in (a). The distance between successive dislocation core is $2d$. See text for details.

mass propels the current venture to unveil its signatures on the emergent electronic bands along GBs in HOTIs.

Key results. We show that the GB superlattice in both two-dimensional (2D) and three-dimensional (3D) HOTIs harbors a variety of dispersive bands, which are typically placed at finite energies. However, as the Burgers vector of the constituting edge dislocations and the domain wall directions of the WD mass approach each other these dispersive bands come closer, hybridize and finally touch when the \mathbf{b} -vector points toward gapless corners or hinges. The GB then fosters an emergent self-organized metallicity near the zero energy, stemming from an interplay of lattice geometry and momentum space topology. These outcomes are anchored from the Fourier transformation of the defect modes in the GB mini Brillouin zone (BZ), their local density of states (LDOS) in real space lattice with GB defects and the spectral flow of the defect modes with varying WD mass domain wall in 2D (Fig. 2)

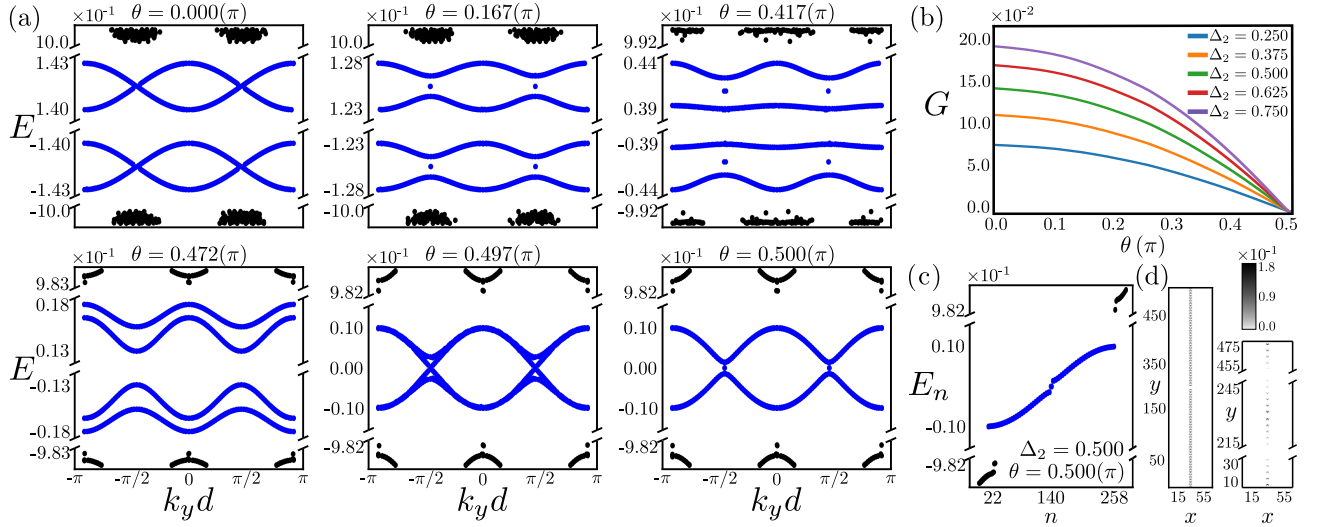


FIG. 2. Grain boundary (GB) in a 2D second-order topological insulator. (a) Evolution of the GB band structure for the defect (blue) and a few bulk (black) modes as a function of θ [Eq. (3)], measuring the relative orientation between the Wilson-Dirac mass domain wall and the dislocation Burgers vector for $\Delta_2 = 0.5$. (b) Band gap (G) between the two closest to zero energy modes, showing that $G \rightarrow 0$ as $\theta \rightarrow \pi/2$, indicating emergent GB metallicity. (c) Energy spectra showing GB modes (blue) and a few bulk modes (black) at $\theta = \pi/2$. (d) Corresponding local density of states of all the GB modes (left) and two zero-energy modes (right), respectively showing their delocalization along the entire GB and near its ends. Results are obtained for a pair of GB and anti-GB (separated by $10a$), each containing 30 (anti)dislocations, with periodic boundaries in all directions.

and 3D (Fig. 3) second-order TIs and 3D third-order TI (Fig. 4). Our results are thus consequential for the quantum crystals ubiquitously hosting GB defects [33], and metamaterials, where such extended defects can be engineered externally [34–37].

Lattice model. The universal Bloch model for HOTIs in two ($D = 2$) and three ($D = 3$) dimensions can be split as $\hat{h}_{\text{HOTI}} = \hat{h}_1 + \hat{h}_\Delta$. The Hamiltonian for the parent first-order TIs takes the form

$$\hat{h}_1 = \sum_{j=1}^D d_j(\mathbf{k})\Gamma_j + M(\mathbf{k})\Gamma_{D+1}, \quad (1)$$

where $d_i(\mathbf{k}) = t \sin(k_i a)$, t is the hopping amplitude set to be unity, and a is the lattice spacing. The first-order WD mass, preserving all non-spatial and crystal symmetries, and featuring band inversion (and thus TIs) within the parameter regime $0 < \Delta_1/B < 4D$, reads

$$M(\mathbf{k}) = \Delta_1 - 2B \left[D - \sum_{j=1}^D \cos(k_j a) \right]. \quad (2)$$

A tower of HOTIs can now be constructed by adding discrete symmetry breaking WD masses (\hat{h}_Δ) to \hat{h}_1 , which can be decomposed as $\hat{h}_\Delta = \hat{h}_2 + \hat{h}_3$. The second-order WD mass in $D = 2$ and $D = 3$ takes the general form [12]

$$\hat{h}_2 = \Delta_2 \{ \cos \theta d_{x^2-y^2}^{\text{lat}} + \sin \theta d_{xy}^{\text{lat}} \} \Gamma_{D+2}, \quad (3)$$

where $0 \leq \theta \leq \pi/2$ (about which more in a moment), $d_{x^2-y^2}^{\text{lat}} = \cos(k_x a) - \cos(k_y a)$, $d_{xy}^{\text{lat}} = \sin(k_x a) \sin(k_y a)$,

and the third-order WD mass (only in $D \geq 3$) reads [38]

$$\hat{h}_3 = \Delta_3 [2 \cos(k_z a) - \cos(k_x a) - \cos(k_y a)] \Gamma_{D+3}. \quad (4)$$

Here $\Gamma_1, \dots, \Gamma_D, \Gamma_{D+1}, \Gamma_{D+2}$ are mutually anticommuting Hermitian matrices each of which squares to unity. Results are independent of their explicit representation.

When $\Delta_3 = 0$, the Bloch Hamiltonian $\hat{h}_1 + \hat{h}_2$ describes a second-order TI in both $D = 2$ and $D = 3$, since \hat{h}_2 gaps out the topological edge (surface) states accommodated by the first-order phase, and leaves only four corners (four z -directional hinges and two xy surfaces) gapless. As such, this mass term for each value of the parameter $0 \leq \theta \leq \pi/2$ features a domain wall, which lies along the principal axes $k_x = 0$ and $k_y = 0$ (the diagonals $k_y = \pm k_x$) for $\theta = \pi/2$ ($\theta = 0$). Sharp corner or hinge modes then appear only when they lie on the axes of inversion (domain wall) for the WD mass (\hat{h}_2) [12].

Since $\hat{h}_1 + \hat{h}_2$ involves four (five) mutually anticommuting Γ matrices in $D = 2$ ($D = 3$), their dimensionality is *four*. Consequently, the corner modes are pinned at zero energy due to a unitary (generated by Γ_5) and an antiunitary particle-hole (PH) symmetry in $D = 2$, while in $D = 3$ only an antiunitary PH symmetry pins hinge modes to zero energy [39], as the maximal number of mutually anticommuting four-dimensional Hermitian Γ matrices is *five*. Notice that $\hat{h}_1 + \hat{h}_2$ also enjoys the antiunitary composite $C_4\mathcal{T}$ symmetry, a product of the four-fold rotation about the z -axis (C_4), generated by $i\Gamma_1\Gamma_2$ and under which $(k_x, k_y) \rightarrow (k_y, -k_x)$, and the time-reversal (\mathcal{T}) in both $D = 2$ and $D = 3$. The explicit

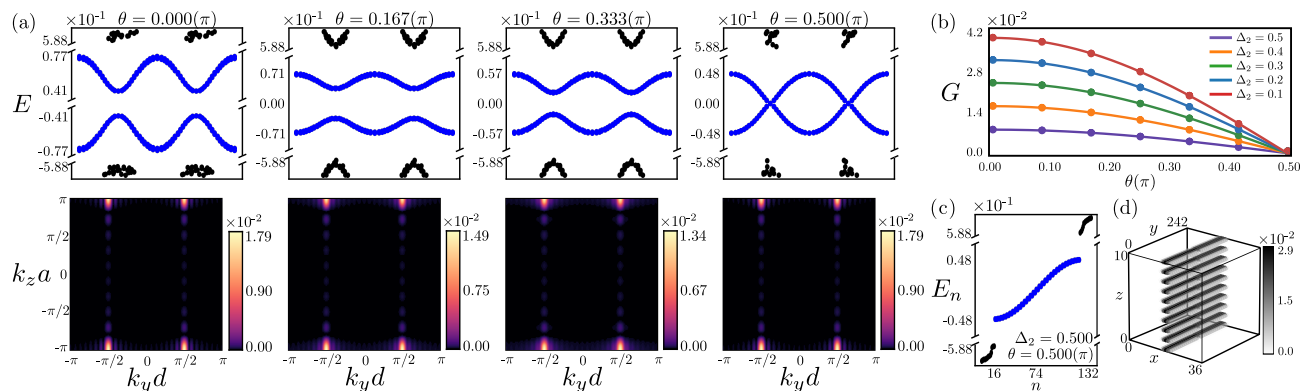


FIG. 3. Grain boundary (GB) in a 3D second-order topological insulator. (a) Evolution of the GB band structure for the defect (blue) and a few bulk (black) modes as a function of θ [Eq. (3)] for $\Delta_2 = 0.5$, with the spectral weight of the two closest to zero energy modes localized at momenta $(\pm\pi/(2d), \pi/a)$ for any θ . (b) Scaling of the gap (G) between two closest to zero energy modes with θ . It vanishes at $\theta = \pi/2$, indicating emergent GB metallicity. (c) Energy spectra showing gapless GB modes (blue) and gapped bulk modes (black). (d) Local density of states for the GB states displaying confinement to the GB plane, on which they are completely delocalized within the 3D bulk, thus yielding a 2D topological metal. Results are obtained for a pair of GB and anti-GB (separated by $10a$), each containing 15 (anti)dislocations, with periodic boundaries in all directions.

forms of the antiunitary PH and \mathcal{T} symmetry generators however depend on the Γ matrix representation.

When we turn on the mass term \hat{h}_3 , the Hamiltonian $\hat{h}_1 + \hat{h}_2 + \hat{h}_3$ (with finite Δ_2 and Δ_3) describes a third-order topological insulator in $D = 3$. Since it features *six* mutually anticommuting Γ matrices, they must therefore be at least eight-dimensional. The additional mass term (\hat{h}_3) gaps out otherwise gapless hinge and xy (top and bottom) surface states, yielding the eight zero-energy corner-localized modes in the cubic geometry. For the sharp corner localization, eight corners of the cubic lattice must coincide with the directions along which $\hat{h}_2 = 0 = \hat{h}_3$ [40]. The corner modes in a third-order TI are pinned at zero energy due to a unitary (generated by Γ_7) as well as an antiunitary PH symmetry.

Since HOTIs are obtained as descendants of the first-order TIs upon systematically switching on the discrete symmetry breaking WD masses (\hat{h}_2 and \hat{h}_3), in what follows, we consider the translationally active M and R phases of the 2D and 3D first-order TIs, respectively, featuring band inversion at finite momentum (\mathbf{K}_{inv}) $\mathbf{M} = (1, 1)\pi/a$ and $\mathbf{R} = (1, 1, 1)\pi/a$ points in the corresponding BZ of the parent square and cubic lattices. For numerical calculations in $D = 2$ and $D = 3$, we throughout set $\Delta_1/B = 6$ and $\Delta_1/B = 11$, respectively [Eq. (2)].

GB: Construction. When introduced in a TI, the elementary building block of a GB defect, a single dislocation, sources an effective hopping phase across the defect $\Phi_{\text{dis}} = \mathbf{K}_{\text{inv}} \cdot \mathbf{b} \pmod{2\pi}$ [1, 3]. Therefore, electrons encircling the defect can pick up a nontrivial hopping phase $\Phi_{\text{dis}} = \pi$ in the M (R) phase on the square (cubic) lattice, while $\Phi_{\text{dis}} = 0$ always in the Γ phase as $\mathbf{K}_{\text{inv}} = 0$ therein. As a result, in a translationally-active first-order phase, a single dislocation hosts localized modes at zero energy. By contrast, in HOTIs the additional higher-

order WD masses typically gap out the dislocation modes and place them at finite energies, unless the Burgers vector pierces a gapless lower-dimensional boundary, while retaining their topological and symmetry protection [12].

When a GB is immersed in a parent translationally-active first-order TI, the localized modes at individual dislocations hybridize, giving rise to an emergent topological metal along the GB superlattice [19]. The emergence of such a self-organized topological metal can be corroborated from the Fourier transform of the GB modes with respect to the superlattice periodicity d , yielding a band structure in the superlattice mini BZ. As the dislocation modes, when hybridize, also develop a comparable weight at the middle of two successive defect cores, we denote the distance between them by $2d$ (Fig. 1). Next, we report the nature of emergent metallic states in the GB defect consisting of edge dislocations in both 2D (Fig. 2) and 3D (Fig. 3) second-order TIs, and 3D third-order TI (Fig. 4), showcasing an intriguing interplay between the defect geometry and the topology of discrete symmetry breaking WD masses (\hat{h}_2 and \hat{h}_3). For concreteness, throughout the Burgers vector of constituting dislocation in the GB is taken to be $\mathbf{b} = a\mathbf{e}_x$. Here we consider only small angle GBs, characterized by $\varphi = \sin^{-1}(a/(2d)) \approx 14.47^\circ (< 15^\circ)$ for $d = 2a$.

GB in 2D second-order TI. The evolution of the GB band structure as the orientation (θ) of the WD mass domain wall is varied with respect to \mathbf{b} is shown in Fig. 2(a). When $\theta = 0$, the axes of inversion for the second-order WD mass (\hat{h}_2) is *perpendicular* to \mathbf{b} , and a single dislocation features PH symmetric localized modes at finite energies [12]. Hybridization among them then yields isolated dispersive bands centered at finite energies along the GB superlattice, separated by a gap G [Fig. 2(b)]. It measures the energy difference between the bottom and

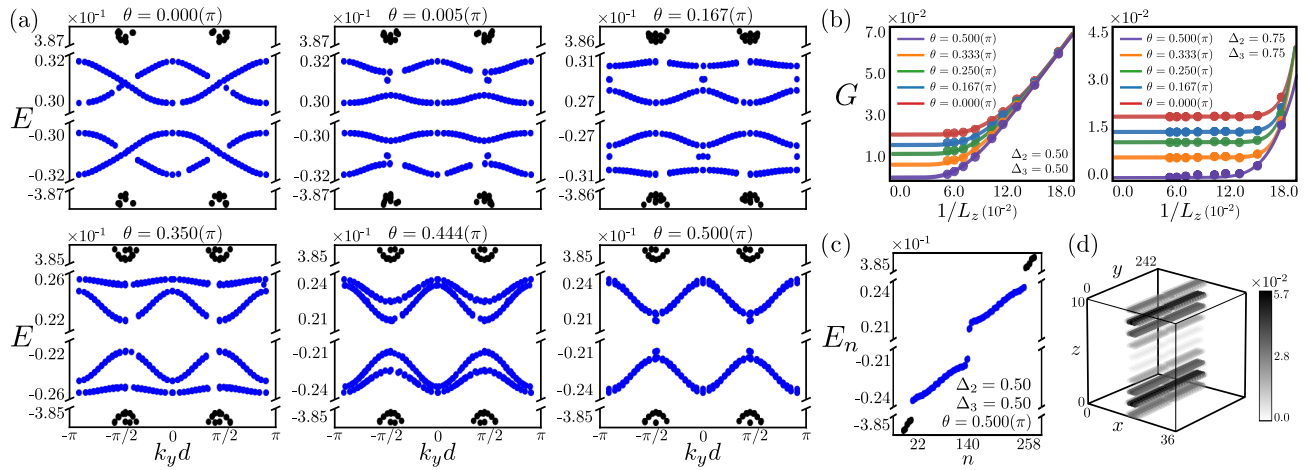


FIG. 4. Grain boundary (GB) in a 3D third-order topological insulator. (a) Evolution of the band-structure on the top and the bottom edges of the GB plane as the orientation of the second-order mass domain wall moves towards principal crystalline axes $\theta = \pi/2$ [Eq. (3)] for $\Delta_2 = \Delta_3 = 0.5$. (b) The gap (G) between the closest to zero energy states as a function of θ for two choices of the Wilson-Dirac mass amplitudes (Δ_2 and Δ_3), showing that $G \rightarrow 0$ as $\theta \rightarrow \pi/2$ (indicating emerging metallicity), but only when the system thickness in the z direction $L_z \rightarrow \infty$. For $\theta = \pi/2$, we show the (c) energy spectra supporting the GB modes (blue) and a few bulk modes (black) and (d) local density of states of the GB modes, showing its strong localization near the top and bottom edges of the GB. Results are obtained for a pair of GB and anti-GB (separated by $10a$), each containing 13 (anti)dislocations, with open (periodic) boundary condition(s) in the z (x and y) direction(s).

top of such dispersive bands living within the conduction and valence bands, respectively. As $\theta \rightarrow \pi/2$, these bands come close to each other and start to hybridize. For $\theta \approx \pi/2$, when the domain wall of \hat{h}_2 is *parallel* to \mathbf{b} , this gap eventually closes, yielding an emergent metal around the zero energy. For any θ , the dispersive or metallic states are always separated from the bulk states, like their parent dislocation modes. For $\theta = \pi/2$, besides the dispersive metallic states a pair of zero-energy modes also appear in the spectra [Fig. 2(a) and (c)]. All of them are *delocalized* along the GB, but confined in its close vicinity, as shown from their LDOS in Fig. 2(d).

GB in 3D second-order TI. In $D = 3$, a GB consists of an array of edge dislocations, which forms a plane spanned by the directions of the dislocation line and the dislocation array, respectively in the z -axis and y -axis for $\mathbf{b} = a\mathbf{e}_x$. Each dislocation line then hosts localized modes along the z direction, which are typically at finite energies for $\theta \neq \pi/2$, unless \mathbf{b} points toward gapless hinges for $\theta = \pi/2$, when the dislocation modes become gapless [12]. These modes, when hybridize, yield a plethora of 2D dispersive bands along the GB defect, manifesting a gap depending on the parameter θ , as shown in the upper panel of Fig. 3(a), with the metallic band structure centered around the zero energy emerging for $\theta = \pi/2$. Furthermore, as shown in the lower panel of Fig. 3(a), the closest to zero-energy modes feature almost the entire spectral weight at momenta $(\pm\pi/(2d), \pi/a)$, which is independent of the parameter θ . The emergent metallicity around the zero energy is further corroborated from the θ -dependence of the gap (G) between bot-

tom and top of the dispersive bands respectively residing within the conduction and valence bands, showing that G goes to zero as $\theta \rightarrow \pi/2$ [Fig. 3(b)]. The GB modes are always well separated from the bulk states for any θ [Fig. 3(a)], which we also explicitly show for $\theta = \pi/2$ in Fig. 3(c). Finally, these modes are highly localized in the yz -plane constituted by the GB (for any θ), as explicitly shown from their LDOS for $\theta = \pi/2$ in Fig. 3(d). Appearance of two gapless Dirac points at $(\pm\pi/(2d), \pi/a)$ when $\theta = \pi/2$ in a 2D GB mini BZ conforms to the Nielsen-Ninomiya Fermion doubling theorem [41].

GB in 3D third-order TI. An edge dislocation in a 3D third-order TI harbors modes localized near its ends on the top and bottom surfaces, for example, when $\mathbf{b} = a\mathbf{e}_x$, which are at finite energies, unless the Burgers vector points toward eight gapless corners, when they become gapless [12]. Consequently, a GB in a 3D third-order TI is expected to host gapped dispersive bands localized near the top and the bottom edges of the defect, which become gapless only when $\theta = \pi/2$. Indeed Fig. 4(a) confirms it, showing that the gap between the dispersive GB bands decreases as the WD mass domain wall approaches the principal crystallographic axes ($\theta \rightarrow \pi/2$), when it should become gapless. A *small* residual gap between these dispersive modes at $\theta = \pi/2$ is purely due to a finite thickness of the system in the z -direction (L_z), which approaches zero as $L_z \rightarrow \infty$. See Fig. 4(b). The GB modes (gapped dispersive or gapless metallic) are always well-separated from the bulk states [Fig. 4(a)], as explicitly shown in Fig. 4(c) and localized near the top and bottom surfaces, as shown in Fig. 4(d) for $\theta = \pi/2$.

Discussion & outlook. Here we show that both 2D and 3D HOTIs foster a variety of dispersive states within the conduction and valence bands of the emergent BZ constituted by the GB superlattice, with the gap between them tunable by the relative orientation of the HOT mass domain wall and the Burgers vector of individual dislocations. Especially, when the Burgers vector pierces gapless corners and hinges, these dispersive states touch each other at zero energy, giving birth to self-organized topological metals confined to the GB defect. See Figs. 2-4.

While here we focus on small angle GBs, described by an array of dislocations (Fig. 1), at large opening angles ($\varphi > 15^\circ$) a GB defect may be described as an array of elementary disclination defects [42] or in terms of a lattice of partial dislocations with stacking faults [43]. As a single disclination [44, 45] and a partial dislocation [46] defect can also harbor localized topological modes, the possibility of emergent metallicity on high-angle GBs stands as a fascinating avenue for future investigation.

The prerequisite for the realization of the proposed emergent metallicity along the GB in HOTIs is a band-inversion at a finite momentum in the BZ (translationally active) such that $\mathbf{K}_{\text{inv}} \cdot \mathbf{b} = \pi$ (modulo 2π), as GB defects are rather ubiquitous in quantum crystals. We emphasize that a metallic behavior has been recently observed at GBs in 1T'-MoTe₂ [33], while some of the realized HOTIs are of translationally-active type [47, 48], which should motivate further investigation of the materials prospects for the realization of our proposal. On the other hand, in metamaterials the predicted GB band structures can be engineered by artificially tuning the tunneling processes and manipulating defects therein. Among them designer metamaterials [34], topoelectric circuits [35, 36], photonic [37] and mechanical [49] lattices are the most promising platforms. Our findings should therefore motivate experimental efforts for the realization of the defect-based emergent band structures in a wide range of both quantum and classical topological materials.

Acknowledgments. D.J.S. and B.R. were supported by NSF CAREER Grant no. DMR- 2238679 of B.R. V.J. acknowledges support of the Swedish Research Council (VR 2019-04735) and Fondecyt (Chile), Grant No. 1230933. Nordita is partially supported by Nordforsk.

[1] Y. Ran, Y. Zhang, and A. Vishwanath, One-dimensional topologically protected modes in topological insulators with lattice dislocations, *Nat. Phys.* **5**, 298 (2009).
 [2] J. C. Y. Teo and C. L. Kane, Topological defects and gapless modes in insulators and superconductors, *Phys. Rev. B* **82**, 115120 (2010).
 [3] V. Juričić, A. Mesáros, R.-J. Slager, and J. Zaanen, Universal Probes of Two-Dimensional Topological Insulators: Dislocation and π Flux, *Phys. Rev. Lett.* **108**, 106403 (2012).

[4] D. Asahi and N. Nagaosa, Topological indices, defects, and Majorana fermions in chiral superconductors, *Phys. Rev. B* **86**, 100504 (2012).
 [5] T. L. Hughes, H. Yao, and X.-L. Qi, Majorana zero modes in dislocations of Sr₂RuO₄, *Phys. Rev. B* **90**, 235123 (2014).
 [6] R.-J. Slager, A. Mesáros, V. Juričić, and J. Zaanen, Interplay between electronic topology and crystal symmetry: Dislocation-line modes in topological band insulators, *Phys. Rev. B* **90**, 241403 (2014).
 [7] T. Nag and B. Roy, Anomalous and normal dislocation modes in Floquet topological insulators, *Commun. Phys.* **4**, 157 (2021).
 [8] S. K. Das and B. Roy, Dynamic melting and condensation of topological dislocation modes, [arXiv:2210.15661](https://arxiv.org/abs/2210.15661).
 [9] A. Panigrahi, R. Moessner, and B. Roy, Non-Hermitian dislocation modes: Stability and melting across exceptional points, *Phys. Rev. B* **106**, L041302 (2022).
 [10] A. Panigrahi, V. Juričić, and B. Roy, Projected topological branes, *Commun. Phys.* **5**, 230 (2022).
 [11] L.-H. Hu and R.-X. Zhang, Dislocation Majorana Bound States in Iron-based Superconductors, [arXiv:2207.10113](https://arxiv.org/abs/2207.10113).
 [12] B. Roy and V. Juričić, Dislocation as a bulk probe of higher-order topological insulators, *Phys. Rev. Res.* **3**, 033107 (2021).
 [13] H. Hamasaki, Y. Tokumoto, and K. Edagawa, Dislocation conduction in Bi-Sb topological insulators, *Appl. Phys. Lett.* **110**, 092105 (2017).
 [14] A. K. Nayak, J. Reiner, R. Queiroz, H. Fu, C. Shekhar, B. Yan, C. Felser, N. Avraham, and H. Beidenkopf, Resolving the topological classification of bismuth with topological defects, *Sci. Adv.* **5**, eaax6996 (2019).
 [15] H. Xue, D. Jia, Y. Ge, Y.-J. Guan, Q. Wang, S.-Q. Yuan, H.-X. Sun, Y. D. Chong, and B. Zhang, Observation of Dislocation-Induced Topological Modes in a Three-Dimensional Acoustic Topological Insulator, *Phys. Rev. Lett.* **127**, 214301 (2021).
 [16] L. Ye, C. Qiu, M. Xiao, T. Li, J. Du, M. Ke, and Z. Liu, Topological dislocation modes in three-dimensional acoustic topological insulators, *Nat. Commun.* **13**, 508 (2022).
 [17] A. Sutton and R. Balluffi, *Interfaces in Crystalline Materials* (Oxford University Press, Oxford, UK, 2007).
 [18] J. Han, S. L. Thomas, and D. J. Srolovitz, Grain-boundary kinetics: A unified approach, *Prog. Mater. Sci.* **98**, 386 (2018).
 [19] R.-J. Slager, V. Juričić, V. Lahtinen, and J. Zaanen, Self-organized pseudo-graphene on grain boundaries in topological band insulators, *Phys. Rev. B* **93**, 245406 (2016).
 [20] M. Amundsen and V. Juričić, Grain-boundary topological superconductor, [arXiv:2212.14038](https://arxiv.org/abs/2212.14038).
 [21] D. J. Salib and B. Roy, Dynamic metal along grain boundaries in Floquet topological crystals, [arXiv:2212.08060](https://arxiv.org/abs/2212.08060).
 [22] W. A. Benalcazar, B. A. Bernevig, and T. L. Hughes, Quantized electric multipole insulators, *Science* **357**, 61 (2017).
 [23] W. A. Benalcazar, B. A. Bernevig, and T. L. Hughes, Electric multipole moments, topological multipole moment pumping, and chiral hinge states in crystalline insulators, *Phys. Rev. B* **96**, 245115 (2017).
 [24] Z. Song, Z. Fang, and C. Fang, ($d - 2$)-Dimensional Edge States of Rotation Symmetry Protected Topological States, *Phys. Rev. Lett.* **119**, 246402 (2017).

- [25] J. Langbehn, Y. Peng, L. Trifunovic, F. von Oppen, and P. W. Brouwer, Reflection-Symmetric Second-Order Topological Insulators and Superconductors, *Phys. Rev. Lett.* **119**, 246401 (2017).
- [26] F. Schindler, A. M. Cook, M. G. Vergniory, Z. Wang, S. S. P. Parkin, B. A. Bernevig, and T. Neupert, Higher-order topological insulators, *Sci. Adv.* **4**, eaat0346 (2018).
- [27] E. Khalaf, Higher-order topological insulators and superconductors protected by inversion symmetry, *Phys. Rev. B* **97**, 205136 (2018).
- [28] C.-H. Hsu, P. Stano, J. Klinovaja, and D. Loss, Majorana Kramers Pairs in Higher-Order Topological Insulators, *Phys. Rev. Lett.* **121**, 196801 (2018).
- [29] A. Matsugatani and H. Watanabe, Connecting higher-order topological insulators to lower-dimensional topological insulators, *Phys. Rev. B* **98**, 205129 (2018).
- [30] Z. Wang, B. J. Wieder, J. Li, B. Yan, and B. A. Bernevig, Higher-Order Topology, Monopole Nodal Lines, and the Origin of Large Fermi Arcs in Transition Metal Dichalcogenides XTe_2 ($X = Mo, W$), *Phys. Rev. Lett.* **123**, 186401 (2019).
- [31] L. Trifunovic and P. W. Brouwer, Higher-Order Bulk-Boundary Correspondence for Topological Crystalline Phases, *Phys. Rev. X* **9**, 011012 (2019).
- [32] D. Călugăru, V. Juričić, and B. Roy, Higher-order topological phases: A general principle of construction, *Phys. Rev. B* **99**, 041301 (2019).
- [33] H. W. Kim, S.-H. Kang, H.-J. Kim, K. Chae, S. Cho, W. Ko, S. Jeon, S. H. Kang, H. Yang, S. W. Kim, S. Park, S. Hwang, Y.-K. Kwon, and Y.-W. Son, Symmetry dictated grain boundary state in a two-dimensional topological insulator, *Nano Lett.* **20**, 5837 (2020).
- [34] S. N. Kempkes, M. R. Slot, J. J. van den Broeke, P. Capiod, W. A. Benalcazar, D. Vanmaekelbergh, D. Bercioux, I. Swart, and C. Morais Smith, Robust zero-energy modes in an electronic higher-order topological insulator, *Nat. Mater.* **18**, 1292 (2019).
- [35] S. Imhof, C. Berger, F. Bayer, J. Brehm, L. W. Molenkamp, T. Kiessling, F. Schindler, C. H. Lee, M. Greiter, T. Neupert, and R. Thomale, Topoelectrical-circuit realization of topological corner modes, *Nat. Phys.* **14**, 925 (2018).
- [36] J. Dong, V. Juričić, and B. Roy, Topoelectric circuits: Theory and construction, *Phys. Rev. Res.* **3**, 023056 (2021).
- [37] F.-F. Li, H.-X. Wang, Z. Xiong, Q. Lou, P. Chen, R.-X. Wu, Y. Poo, J.-H. Jiang, and S. John, Topological light-trapping on a dislocation, *Nat. Commun.* **9**, 2462 (2018).
- [38] T. Nag, V. Juričić, and B. Roy, Hierarchy of higher-order Floquet topological phases in three dimensions, *Phys. Rev. B* **103**, 115308 (2021).
- [39] B. Roy, Antiunitary symmetry protected higher-order topological phases, *Phys. Rev. Res.* **1**, 032048 (2019).
- [40] B. Roy and V. Juričić, Mixed-parity octupolar pairing and corner Majorana modes in three dimensions, *Phys. Rev. B* **104**, L180503 (2021).
- [41] H. Nielsen and M. Ninomiya, Absence of neutrinos on a lattice: (I). Proof by homotopy theory, *Nucl. Phys. B* **185**, 20 (1981).
- [42] A. A. Nazarov, O. A. Shenderova, and D. W. Brenner, Elastic models of symmetrical $\langle 001 \rangle$ and $\langle 011 \rangle$ tilt grain boundaries in diamond, *Phys. Rev. B* **61**, 928 (2000).
- [43] A. H. King and F.-R. Chen, Interactions between lattice partial dislocations and grain boundaries, *Mater. Sci. Eng.* **66**, 227 (1984).
- [44] W. A. Benalcazar, T. Li, and T. L. Hughes, Quantization of fractional corner charge in C_n -symmetric higher-order topological crystalline insulators, *Phys. Rev. B* **99**, 245151 (2019).
- [45] M. Geier, I. C. Fulga, and A. Lau, Bulk-boundary-defect correspondence at disclinations in rotation-symmetric topological insulators and superconductors, *SciPost Phys.* **10**, 092 (2021).
- [46] R. Queiroz, I. C. Fulga, N. Avraham, H. Beidenkopf, and J. Cano, Partial Lattice Defects in Higher-Order Topological Insulators, *Phys. Rev. Lett.* **123**, 266802 (2019).
- [47] F. Schindler, Z. Wang, M. G. Vergniory, A. M. Cook, A. Murani, S. Sengupta, A. Y. Kasumov, R. Deblock, S. Jeon, I. Drozdov, H. Bouchiat, S. Guéron, A. Yazdani, B. A. Bernevig, and T. Neupert, Higher-order topology in bismuth, *Nat. Phys.* **14**, 918 (2018).
- [48] R. Noguchi, M. Kobayashi, Z. Jiang, K. Kuroda, T. Takahashi, Z. Xu, D. Lee, M. Hirayama, M. Ochi, T. Shirasawa, P. Zhang, C. Lin, C. Bareille, S. Sakuragi, H. Tanaka, S. Kunisada, K. Kurokawa, K. Yaji, A. Harasawa, V. Kandyba, A. Giampietri, A. Barinov, T. K. Kim, C. Cacho, M. Hashimoto, D. Lu, S. Shin, R. Arita, K. Lai, T. Sasagawa, and T. Kondo, Evidence for a higher-order topological insulator in a three-dimensional material built from van der Waals stacking of bismuth-halide chains, *Nat. Mater.* **20**, 473 (2021).
- [49] I. H. Grinberg, M. Lin, W. A. Benalcazar, T. L. Hughes, and G. Bahl, Trapped State at a Dislocation in a Weak Magnetomechanical Topological Insulator, *Phys. Rev. Appl.* **14**, 064042 (2020).